Preparation and in-Situ Spectroscopic Characterization of Molecularly Dispersed Titanium Oxide on Silica

Xingtao Gao,[†] Simon R. Bare,[‡] J. L. G. Fierro,[§] Miguel A. Banares,[§] and Israel E. Wachs*[,†]

Department of Chemistry and Chemical Engineering, Zettlemoyer Center for Surface Studies, Lehigh University, 7 Asa Drive, Bethlehem, Pennsylvania 18015; UOP Research, Des Plaines, Illinois 60017; and Institute de Catalisis y Petroleoquimica, C.S.I.C., Campus Univeritario Cantoblanco, E-28049-Madrid, Spain

Received: March 10, 1998

The molecularly dispersed TiO_2/SiO_2 supported oxides were prepared by the incipient wetness impregnation of 2-propanol solutions of titanium isopropoxide. Experimental monolayer dispersion of surface titanium oxide species on SiO_2 was reached at ∼4 Ti atoms/nm^2 with a two-step impregnation procedure. The surface structures of the molecularly dispersed TiO_2/SiO_2 under various environments were extensively investigated by in-situ spectroscopic techniques (e.g., Raman, UV−vis−NIR DRS, and XANES) as well as XPS. The combined characterization techniques revealed the consumption of surface Si−OH groups and the formation of Ti−O−Si bridging bonds. In the dehydrated state, the surface Ti atoms in the 1% TiO_2/SiO_2 sample (0.24 Ti atoms/nm^2) are predominantly found to be isolated TiO_4 units, whereas at maximum surface coverage (∼4 Ti atoms/nm^2), two-dimensional polymerized TiO_5 units are dominant on the silica surface. The in-situ spectroscopic studies demonstrated that the coordination and ligands of the surface Ti cations change upon hydration/dehydration as well as during methanol oxidation. Methanol oxidation showed that the molecularly dispersed surface titanium oxide species exhibit completely different catalytic behavior (predominantly redox products) compared to bulk titanium oxide (predominantly dehydration products). Furthermore, the TOF of the surface titanium oxide species is strongly dependent on their local structures and varies by 1 order of magnitude (isolated $TiO_4 \gg$ polymerized TiO_5). These new results provide fundamental insights about molecular structure−reactivity/selectivity relationships of the molecularly dispersed TiO_2/SiO_2 supported oxides.

Introduction

To improve the mechanical strength, thermal stability, and surface area of TiO_2, TiO_2/SiO_2 supported oxides have been considered as advanced support materials as substitutes for pure TiO_2.[1−6] Titanium oxide modified silica takes advantage of the properties of TiO_2 (an n-type semiconductor and an active catalytic support) and SiO_2 (large surface area, high thermal stability, and good mechanical strength) as the catalyst support[4−6] and extends its applications as a catalyst through the generation of new catalytic active sites.[7−9]

The utility and applications of metal oxides on silica have driven research toward the production of catalysts that have a high percentage of the metal oxide in a dispersed state (two-dimensional surface metal oxide overlayer).[10−13] It is well-known that the silica surface is quite inert and that it is very difficult to synthesize highly dispersed metal oxides on the silica surface. Of all the different chemical modification reactions on silica, the surface hydroxyls generally act as the adsorptive/reactive sites because of their hydrophilic character. Thus, the preparation of highly dispersed metal oxides on silica by either impregnation or chemical vapor deposition often involves a highly reactive H-sequestering precursor, such as $TiCl_4$ or titanium alkoxides, which will readily react with the surface hydroxyls of the silica support.[1,2,14−18] Two types of Ti oxide species, i.e., highly dispersed surface TiO_x species and TiO_2 crystallites, can be present on the silica surface, and their relative amounts depend on the preparation conditions and chemical compositions (surface Ti densities).[1,2,16] Raman spectroscopy was employed to examine the maximum dispersion in this work since the identification of the dispersed TiO_x species is difficult with bulk characterization techniques such as XRD. It has been shown that Raman spectroscopy is extremely sensitive to the formation of crystalline TiO_2 with a minimum detectable amount of 0.05 wt %TiO_2.[19] In the present work, factors that control the maximum surface coverage of titanium oxide on silica are investigated.

The physicochemical and reactivity/selectivity properties of oxide catalysts are often a strong function of their structural characteristics. Extensive investigations have been conducted on Ti silicalites and TiO_2-SiO_2 mixed oxides.[20,21] In both materials, Ti atoms are shown to substitute Si in the silica framework or matrix to form tetrahedral TiO_4 units, which function as active sites for epoxidation reactions. The highly dispersed TiO_2/SiO_2 supported oxides have also been shown to be active for liquid-phase epoxidation reactions.[7,8] However, the structural characteristics of TiO_2/SiO_2 supported oxides and their relationship with the physicochemical and reactivity/selectivity properties are poorly understood due to the lack of systematic fundamental studies. Therefore, the present investigation focuses on the in-situ molecular structural characterization of the highly dispersed TiO_2/SiO_2 under various conditions with several different molecular spectrocopies: Raman spectroscopy, UV−vis−NIR DRS, and XANES spectroscopy. The structural information derived from these in-situ spectroscopic studies provide fundamental understanding about the interaction of titanium oxide with the silica surface and demonstrate that the molecular structure of the highly dispersed TiO_x species on

* To whom correspondence should be addressed.
[†] Lehigh University.
[‡] UOP Research.
[§] Campus Univeritario Cantoblanco.

S1089-5647(98)01423-0 CCC: $15.00
Published on Web 06/26/1998

silica is sensitive to the environmental conditions. Furthermore, methanol oxidation as a probe reaction was employed to examine the reactivity of the highly dispersed TiO_2/SiO_2 catalysts since this reaction is often used to distinguish between acid sites and redox sites on oxide catalysts.[22] This fundamental result is used to develop the molecular structure−reactivity/selectivity relationships of TiO_2/SiO_2 catalysts.

Experimental Section

1. Catalyst Preparation. The silica support used for this study was Cabosil EH-5. This fluffy material was treated with water in order to condense its volume for easier handling. Then the wet SiO_2 was dried at 120 °C and subsequently calcined at 500 °C overnight. The resulting surface area was 332 m^2/g.

The TiO_2/SiO_2 supported oxide catalysts were prepared by the incipient wetness impregnation of 2-propanol solutions of titanium isopropoxide ($Ti(O-Pr^i)_4$, Alfa-Aesar, 99.999% purity). The preparation was performed inside a glovebox with continuously flowing N_2. The SiO_2 support was initially dried at 120 °C to remove the physisorbed water before impregnation. After impregnation at room temperature, the samples were kept inside the glovebox with flowing N_2 for overnight. The samples were subsequently dried at 120 °C in flowing N_2 for 1 h and calcined at 500 °C in flowing air for 4 h. A two-step preparation procedure was employed to prepare samples with loadings higher than 8 wt % TiO_2. The second impregnation followed the same procedure described above by using 8% TiO_2/SiO_2 as the starting material to prepare 10%, 12%, and 15% TiO_2/SiO_2 catalysts. Multiple impregnation steps were used to prepare samples with loadings higher than 15% TiO_2. The final catalysts were denoted as *x*% TiO_2/SiO_2. The actual composition of the TiO_2/SiO_2 catalysts was determined by atomic absorption. Samples were dissolved in HF solutions and measured on a Perkin-Elmer system with a sensitivity of 1.9 mg/mL.

The BET surface area of each sample was measured by nitrogen adsorption/desorption isotherms on a Micromeritics ASAP 2000.

2. Raman and FT-IR Spectroscopy. Raman spectra were obtained with the 514.5 nm line of an Ar^+ ion laser (Spectra Physics, model 164). The scattered radiation from the sample was directed into an OMA III (Princeton Applied Research, model 1463) optical multichannel analyzer with a photodiode array cooled thermoelectrically to −35 °C. The exciting laser power was measured at the sample to be about 10−50 mW. The samples were pressed into self-supporting wafers. The Raman spectra of the dehydrated samples were recorded at room temperature and were obtained after heating the sample in flowing O_2 at 450−500 °C for 1 h in a stationary quartz cell.

The in-situ Raman spectra during methanol oxidation were collected in the 2700−3100 cm^{-1} region on a second Raman apparatus with an OMA III detector (Princeton Applied Research, model 1463) and the 514.5 nm line of an Ar^+ ion laser (Spectra Physics, model 165). A self-supporting sample disk of 100−200 mg was mounted on the sample holder, which is capable of spinning inside a quartz cell. The in-situ Raman cell setup was described in detail elsewhere.[23] The sample in the cell was heated at 500 °C for 1 h in a flowing O_2/He (11/6) mixture (Linde Specialty Gas; O_2, 99.99% purity; He, ultrahigh purity). The background Raman spectrum was taken after the sample was cooled to 230 °C. Then, methanol vapor was introduced by passing O_2/He mixture through liquid methanol in an ice bath (4 mol % CH_3OH in the saturated gaseous mixture). The Raman spectra under reaction conditions were obtained after reaching steady state (∼30 min at 230 °C). The Raman spectra after removal of methanol from the feed stream as well as at a higher temperature of 300 °C, with/without methanol in the feed gas, were also recorded in order to examine the stability of the chemisorbed species.

Infrared spectra were only recorded under ambient conditions with a BIO-RAD FTS-40A spectrometer. The samples were mixed with KBr (3/200 by weight) and pressed into thin wafers.

3. X-ray Photoelectron Spectroscopy (XPS). XPS spectra were collected with a Fisons ESCALAB 200R electron spectrometer equipped with a hemispherical electron analyzer and an Mg Kα X-ray source ($h\nu = 1253.6$ eV) powered at 120 W. A PDP 11/05 computer from DEC was used for collecting and analyzing the spectra. The samples were placed in small copper cylinders and mounted on a transfer rod placed in the pretreatment chamber of the instrument. All samples were outgassed at 500 °C before XPS analysis. The binding energies (BE) were referenced to Si_{2p} (BE = 103.4 eV) with an accuracy of ±0.2 eV. The atomic concentration ratios were calculated by correcting the intensity ratios with theoretical sensitivity factors proposed by the manufacturer.

4. UV−vis−NIR Diffuse Reflectance Spectroscopy. Diffuse reflectance spectra (DRS) in the range 200−2200 nm were taken on a Varian Cary 5 UV−vis−NIR spectrophotometer. The spectra were recorded against a halon white reflectance standard as the baseline. The computer processing of the spectra with Bio-Rad Win-IR software consisted of conversion of wavelength (nm) to wavenumber (cm^{-1}) and calculation of the Kubelka−Munk function ($F(R_\infty)$) from the absorbance. Samples were granulated for DRS measurements, and the size fraction of 60−100 mesh was loaded in a quartz flow cell with a Suprasil window. After each treatment, the quartz cell was quickly sealed off and cooled to room temperature for DRS measurements. The spectra of hydrated samples were obtained under ambient conditions. The spectra of partially dehydrated samples were taken after samples were calcined at 120 °C in flowing O_2/He (13/81) for 1 h. The spectra of fully dehydrated samples were obtained after samples were further calcined at 500 °C in flowing O_2/He for 1 h. The DRS spectra for methanol chemisorption were recorded after the dehydrated sample was reacted with a gaseous mixture of CH_3OH/O_2/He (4 mol % CH_3OH in the saturated gaseous mixture) at 230 °C for 30 min.

5. X-ray Absorption Spectroscopy (XANES). The X-ray absorption experiments at the Ti K-edge were performed on beam line X19A at the National Synchrotron Light Source, Brookhaven National Laboratory. The storage ring operated at 2.5 GeV with a current between 200 and 300 mA. The X-rays were monochromatized with an NSLS boomerang-type flat crystal monochromator with Si(111) crystals. The beam is focused and vertically/horizontally collimated using two Rh-coated mirrors. A white beam slit of 1 mm was used. The harmonic content was reduced by detuning the monochromator crystals by 20%. The horizontal and vertical slits were optimized to minimize scattered light. The XAFS spectra were measured in transmission. The incident beam intensity was monitored using an ionization chamber with a constant purge of He, and the transmission ionization chamber was filled with nitrogen. The samples were prepared by grinding each to fine powder and pressing into self-supporting wafers of appropriate thickness. These wafers were held in a quartz in-situ XAFS cell with Kapton windows. The cell was connected to a gas manifold and the temperature controlled using a Eurotherm controller. XANES spectra were initially acquired at room temperature in a He purge and after heating to 500 °C at 10 °C/min in O_2/He (20/80), holding for 30 min at 500 °C, and

TABLE 1: Surface Areas and Compositions of TiO_2/SiO_2 Catalysts

catalyst	surf. area (m^2/g)	wt % TiO_2[a]	surf. density (Ti atom/nm^2)	Ti/Si XPS atomic ratio
SiO_2	332	0.00	0.00	0.000
1% TiO_2/SiO_2	305	1.05	0.24	0.009
5% TiO_2/SiO_2	280	6.58	1.60	0.035
8% TiO_2/SiO_2	253	9.85	2.48	0.061
10% TiO_2/SiO_2	270	10.80	2.75	0.079
12% TiO_2/SiO_2	265	14.75	3.93	0.103
15% TiO_2/SiO_2	229	15.71	4.23	0.105

[a] Actual TiO_2 concentration obtained by atomic absorption.

then cooling to room temperature. During the cooling, the gas was switched to 100% He at 200 °C. The monochromator was calibrated using a Ti foil (4966.0 eV), and periodic energy calibration checks were performed throughout the data acquisition. Two spectra of each sample were recorded, and the data presented are the average spectra.

The XANES spectra were processed using the BAN software package. The energy scale was established by setting the maximum of the first derivative of the XANES spectra of the Ti metal foil to 0.0 eV. The background was approximated by a least-squares fit of the pre-edge region (−90 to −30 eV) and was subtracted from the spectrum. The spectra were normalized to unity absorption by dividing by a least-squares fit of the absorption between 50 and 250 eV above the absorption edge.

6. Catalytic Studies. Methanol oxidation was used to examine the surface reactivity of TiO_2/SiO_2 catalysts. The reaction was carried out in an isothermal fixed-bed differential reactor, which was held vertically and made out of Pyrex glass with 6.2 mm outer diameter. About 60 mg catalyst with a size fraction of 60−100 mesh was tested for methanol oxidation at 290 °C at atmospheric pressure. The reactant gas mixture of $CH_3OH/O_2/He$, molar ratio of ∼6/13/81, was used with a total flow rate of 100 mL/min. The gas feed was controlled by mass flow controllers (Brooks). Analysis of the reactor effluent was performed using an on-line gas chromatograph (HP 5890 series II) equipped with FID and TCD detectors. A Carboxene-1000 packed column and a CP-sil 5CB capillary column were used in parallel for TCD and FID, respectively. The samples were pretreated in a stream of O_2/He gas mixture at 450 °C for 0.5 h before each run. The methanol conversion data were obtained for catalytic runs for 1−2 h.

Results

1. Bulk Compositions and Surface Areas of the TiO_2/SiO_2 Catalysts. The nominal and actual bulk compositions and surface areas of TiO_2/SiO_2 catalysts are shown in Table 1. The actual TiO_2 concentrations of the TiO_2/SiO_2 samples were analyzed by atomic absorption and are slightly in variance with the expected value. Unless otherwise notified, all TiO_2 loadings mentioned in the paper are referred to the nominal values. The surface area of TiO_2/SiO_2 decreases systematically with increasing TiO_2 loading. However, the variation in surface areas between the 5% TiO_2/SiO_2 and 12% TiO_2/SiO_2 samples is relatively small.

2. XPS Surface Analysis. The surface Ti/Si atomic ratios obtained by XPS analysis are also presented in Table 1. The surface Ti/Si ratios were plotted against the bulk Ti/Si atomic ratios calculated from the actual TiO_2 concentration, as shown in Figure 1. It can be seen that the Ti/Si surface and bulk ratios have a linear relationship up to ∼15% TiO_2. However, the slope of this line is even less than 1. Since the silica outer surface must be rich in Ti, the XPS analysis suggests that a majority of the Ti atoms may reside on the surface of inside channels or pores of the silica support that is out of the XPS detection sight.

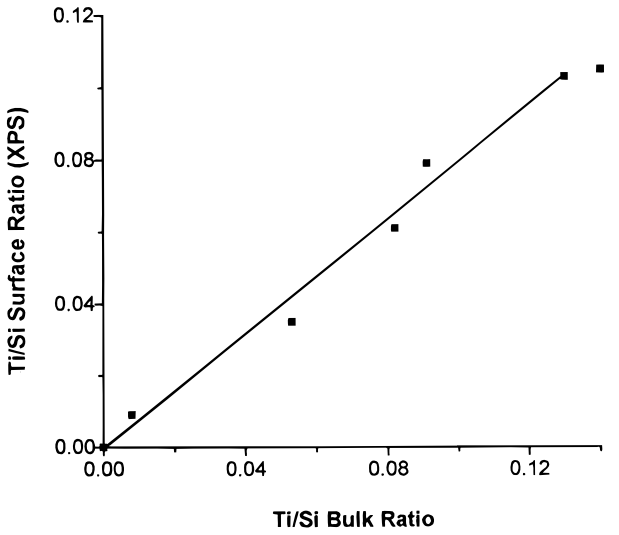

Figure 1. Ti/Si atomic bulk ratio versus Ti/Si atomic surface ratio.

TABLE 2: Binding Energies of Core Electrons for Dehydrated TiO_2/SiO_2 Catalysts

catalysts	O 1s (eV)	Si 2p (eV)	Ti $2p_{3/2}$ (eV)
SiO_2	532.9	103.4	
1% TiO_2/SiO_2	532.9	103.4	459.5
5% TiO_2/SiO_2	532.9	103.4	459.1
8% TiO_2/SiO_2	533.0	103.4	459.0
10% TiO_2/SiO_2	533.0 (89)[a] 531.2 (11)	103.4	458.9
12% TiO_2/SiO_2	532.9 (88) 531.1(12)	103.4	459.0
15% TiO_2/SiO_2	533.0 (78) 531.4 (22)	103.4	458.9
TiO_2	530.7		458.5

[a] The number in parentheses indicates the percentage of the band.

The BE values of Si 2p, Ti $2p_{3/2}$, and O 1s for the dehydrated TiO_2/SiO_2 samples are presented in Table 2. Because of the overwhelming signal from the O 1s band at 533.0 eV due to the SiO_2 support, only up to 10% TiO_2 does a second band at ∼531.2 eV be resolved, and its percentage increases with increasing TiO_2 loading. This new BE band has been ascribed to the oxygen on the Ti−O−Si bridging bond.[2,5,24,25] The relative change on the BE values of Ti $2p_{3/2}$ with respect to SiO_2 can easily be observed as a function of TiO_2 loading since Si 2p was used as the reference. The average Ti $2p_{3/2}$ BE of 1% TiO_2/SiO_2 is the highest, which is 1 eV higher than that of pure TiO_2. For the other TiO_2/SiO_2 samples (15% TiO_2 and below), the BE values of Ti $2p_{3/2}$ are about 0.4−0.6 eV higher than pure TiO_2. The blue shifts of both the O 1s and Ti $2p_{3/2}$ BE values of the TiO_2/SiO_2 samples with respect to pure TiO_2 could be associated with the formation of Ti−O−Si bonds, which result in an increase in the effective positive charge on Ti and a decrease in the effective negative charge on O since the Si atoms are more electronegative and less polarizable than the Ti atoms.[21,24]

3. Raman and FT-IR Spectroscopy. The Raman spectra of the dehydrated SiO_2 and TiO_2/SiO_2 samples are presented in Figure 2. The silica support possesses Raman features at ∼410, ∼487, 607, 802, and ∼976 cm^{-1}. The ∼976 cm^{-1} band is associated with Si−OH stretching mode of the surface hydroxyls, and its intensity decreases with increasing Ti loading. The broad bands at 607 and 487 cm^{-1} are assigned to D2 and D1 defect modes which have been attributed to tri- and

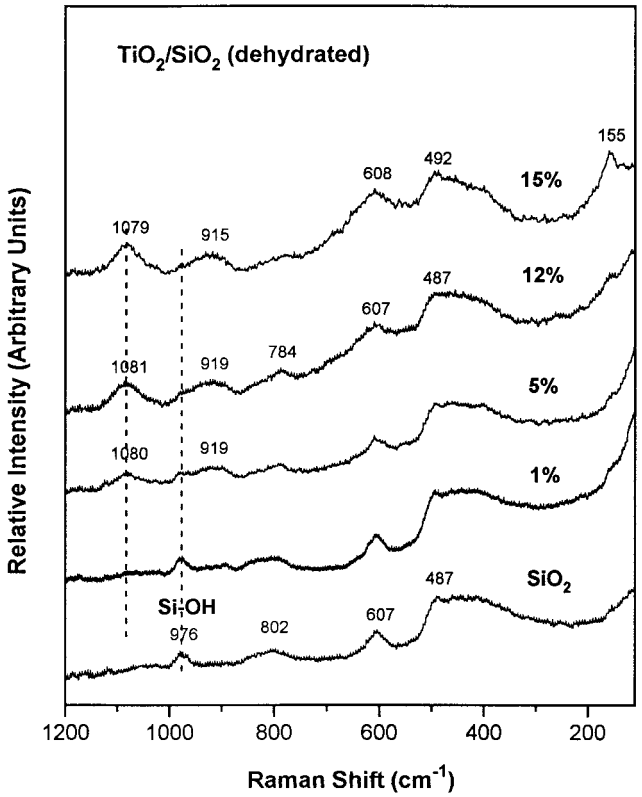

Figure 2. Raman spectra of the dehydrated TiO_2/SiO_2 samples at different loadings.

tetracyclosiloxane rings produced via the condensation of surface hydroxyls.[17,26] The band at ~802 cm^{-1} has been assigned to the symmetrical Si−O−Si stretching mode and the 430−410 cm^{-1} band to the Si−O−Si bending mode.[27] Changes in the silica Raman bands at 607, ~487, and 430−410 cm^{-1} are not very significant up to 12% TiO_2. However, the ~802 cm^{-1} band shifts downward to ~784 cm^{-1} and becomes less broad, suggesting that some Si−O−Si bridges are affected by the dispersed titanium oxide. Two new broad Raman bands are also observed at ~1080 and ~919 cm^{-1}, with the 1080 cm^{-1} band being relatively stronger. These bands have been assigned to silica vibrations perturbed by the presence of Ti, which are indicative of the formation of Ti−O−Si bonds.[9,28] When the TiO_2 loading reaches 15% (actual 15.71% TiO_2), a weak Raman band at ~155 cm^{-1} is observed, which is indicative of the formation of a trace amount of crystalline TiO_2 (anatase). Since the actual TiO_2 loading in the 12% TiO_2/SiO_2 sample is 14.75 wt %, these results indicate that the maximum dispersion on SiO_2 is ~4 Ti atoms/nm^2 (see Table 1). At loadings higher than 15% TiO_2, strong Raman bands due to TiO_2 crystallites (anatase) are observed. However, XRD experiments cannot detect the presence of TiO_2 crystallites (anatase) below 30% TiO_2 loading, suggesting that the TiO_2 crystalline particles on SiO_2 are very small and below the detection sensitivity of the XRD technique (<40 Å). This observation once again demonstrates that Raman spectroscopy is extremely sensitive to the formation of crystalline TiO_2 (anatase) particles.

The Raman spectra of the hydrated TiO_2/SiO_2 samples are shown in Figure 3. Hydration of the samples significantly weakens the Raman band at ~1080 cm^{-1}, while a relatively strong broad band appears at 940~960 cm^{-1}. This new Raman band shifts downward from 955 to 943 cm^{-1} as the Ti loading increases from 5% to 15%, which suggests the connection of this band with the Ti species. The pronounced Raman spectral difference between hydrated and dehydrated states of the TiO_2/SiO_2 samples strongly suggests that the titanium oxide species on SiO_2 are highly dispersed surface species, which are subject to change in surface structure upon hydration/dehydration.

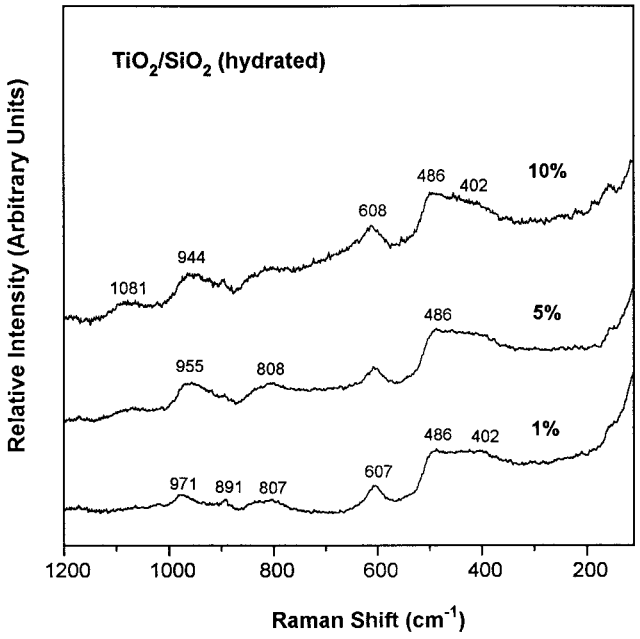

Figure 3. Raman spectra of the hydrated TiO_2/SiO_2 samples at different loadings.

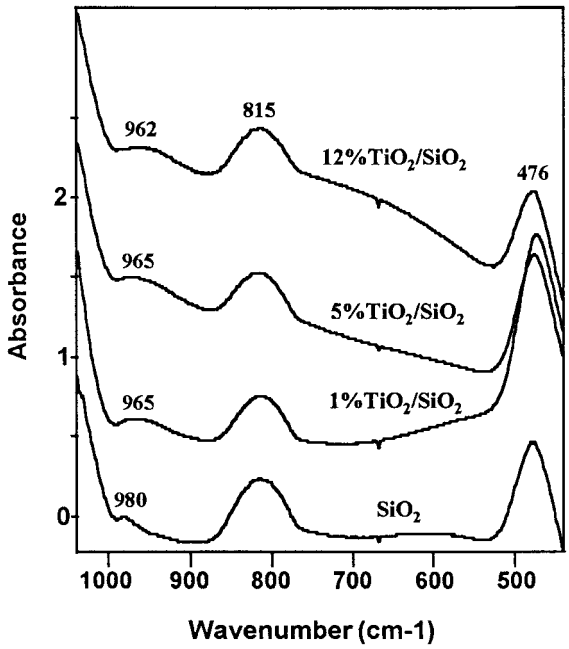

Figure 4. Infrared spectra of the hydrated samples (with KBr).

The FT-IR spectra of SiO_2 and 1%, 5%, and 12% TiO_2/SiO_2 samples are provided in Figure 4. Pure silica exhibits the symmetrical Si−O−Si stretching vibration at ~815 cm^{-1}, along with a very weak band at 980 cm^{-1} due to the symmetric stretch of Si−OH groups.[29,30] The addition of titanium surface oxide species decreases the 980 cm^{-1} band, and a new broad band appears at ~965 cm^{-1}, which is associated with the formation of Ti−O−Si bridges.[31−34] Since the infrared spectra were recorded at ambient conditions with KBr mixture, the results indicate the presence of some Ti−O−Si bonds on the hydrated TiO_2/SiO_2 samples.

Both Raman and FT-IR spectroscopies provide complementary and valuable information about the surface structure of the

hydrated Ti species on the silica support. The new IR band at ~965 cm^{-1} is very weak, especially compared to TiO_2-SiO_2 mixed oxides[31,35] and Ti silicalite,[29] and does not change noticeably with increasing Ti loading. However, the Raman band at 940−960 cm^{-1} is barely observable for the 1% TiO_2/SiO_2 sample, but the band intensity is very strong for the higher loading samples. This result suggests that the Raman band at 940−960 cm^{-1} may not be exactly the same type of vibration as the IR band at ~965 cm^{-1}. The Raman band at 940−960 cm^{-1} may be associated with Si−OH groups perturbed by nearby Ti cations, which result from the hydrolysis of Ti−O−Si bonds. Dehydration causes the disappearance of the Raman band at 940−960 cm^{-1}, and two new Raman bands appear at 1080 and ~919 cm^{-1}. (The relative intensity of the 1080 cm^{-1} band is stronger.) The 1080 cm^{-1} band can also be seen in the hydrated samples, but it is very weak. It is speculated that in the hydrated state the IR band at 965 cm^{-1} may be associated with Ti−O−Si bridging bonds, whereas Raman spectra of the hydrated samples may be ascribed to two types of bonds: the 940−960 cm^{-1} band due to Si−OH···Ti and the 1080 and 919 cm^{-1} bands due to Si−O−Ti bridging bond. In the dehydrated state, it is noted that the Raman band at 1080 cm^{-1} is relatively stronger than the band at 919 cm^{-1}, which is different from the results of Ti silicalites where the band at ~960 cm^{-1} is much stronger than the band at 1115 cm^{-1}.[9] Moreover, the two Raman bands at 1080 and 919 cm^{-1}, if compared with the two Raman bands at 1115 and 960 cm^{-1} in Ti silicalites,[9] are about 40 cm^{-1} lower, suggesting that the Si−O vibration perturbed by surface Ti species (loading higher than 1 wt %TiO_2) may be in a less stressed/rigid state or the average coordination number of Ti cations on the silica surface may be higher than in the Ti silicalite framework. If we assume the band assignment by Deo et al.[9] that the 1080 cm^{-1} band is due to SiO_4 unit containing a single nonbridging oxygen (denoted as ≡SiO···Ti) and the 960 cm^{-1} band due to SiO_4 unit containing two nonbridging oxygens (=$Si(O\cdots Ti)_2$), the relative concentration of ≡SiO···Ti on the surface of TiO_2/SiO_2 supported oxides should be much higher than that in the Ti silicalite framework. It is also interesting to note that the relative intensity of the 919 cm^{-1} band increases as the calcination temperature increases up to 1000 °C (not shown here), suggesting an increase in the =$Si(O\cdots Ti)_2$ concentration due to the shrinking of the silica surface at very high temperature.

The in-situ Raman spectra of 12% TiO_2/SiO_2 during methanol oxidation are presented in Figure 5. Raman bands at ~2953, ~2930, 2854, and 2834 cm^{-1} are observed due to the chemisorption of methanol. The Raman bands at ~2953 and ~2854 cm^{-1} are characteristic of the C−H symmetric stretching vibrations of the surface methoxy species on the silica support (Si−OCH_3),[23] whereas the Raman bands at ~2930 and ~2834 cm^{-1} are most likely associated with the C−H symmetric stretching vibrations of the surface Ti−methoxy groups, similar to those of V−methoxy species at almost identical positions.[23] The Ti−methoxy species on pure TiO_2 (P-25) possess very strong Raman bands at 2920 and 2821 cm^{-1}, which are 10 cm^{-1} lower than the Ti−methoxy species on SiO_2. The surface Ti−methoxy species on SiO_2 are less stable than the Si−methoxy species because the Raman band intensity of the Ti−methoxy species is reduced relative to the Si−methoxy species when methanol is removed from the feed stream.

4. UV−vis−NIR Diffuse Reflectance Spectroscopy. The DRS spectra of 1% TiO_2/SiO_2 sample under hydrated, partially dehydrated, and completely dehydrated conditions are presented in Figure 6. In the near-IR region where the overtone and

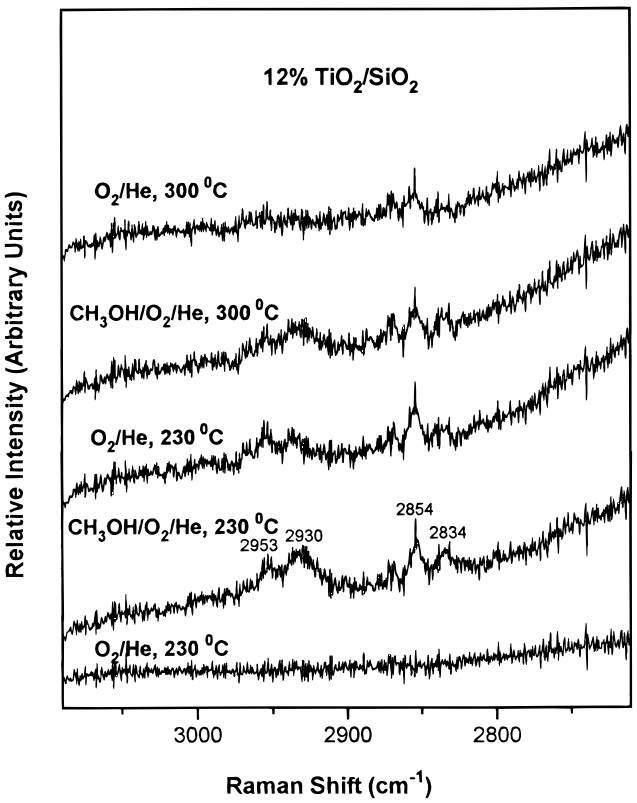

Figure 5. In-situ Raman spectra of the 12% TiO_2/SiO_2 catalyst at various stages of methanol oxidation.

combination bands of hydroxyls are located, the hydrated sample possesses bands at 7315, 7140, 6881, and 5271 cm^{-1}. The 7315 cm^{-1} band can be assigned to the overtone vibration of the isolated Si−OH groups at 3746 cm^{-1}.[30] The bands at 7140, 6881, and 5271 cm^{-1} are associated with physisorbed H_2O molecules on the sample surface under ambient conditions. After partial dehydration at 120 °C, the three IR bands corresponding to physisorbed H_2O molecules simultaneously disappear, which indicates the complete desorption of physisorbed H_2O molecules. However, the intensity of the 7315 cm^{-1} band significantly increases due to the generation of isolated hydroxyl groups from H-bonded hydroxyls, with vibrations around 7100−7300 cm^{-1}, which were initially associated with physisorbed H_2O molecules. Dehydration at 500 °C substantially decreases the band intensity in the 7100−7300 cm^{-1} region, indicating a further decrease in the concentration of the H-bonded hydroxyl groups. In the UV−vis region, the hydrated 1%TiO_2/SiO_2 sample possesses a band at ~46 000 cm^{-1}, which is due to the ligand−metal charge-transfer (LMCT) transitions between Ti^{4+} and oxygen ligands, such as −OH, −O−Si, −O−Ti, or H_2O. A blue shift of ~800 cm^{-1} was observed after partial dehydration at 120 °C. Complete dehydration at 500 °C further upward shifts the peak position to 47 600 cm^{-1}. For the well-documented Ti silicalite (TS-1), the absorption band observed at 50 000−48 000 cm^{-1} has been assigned to the LMCT transitions of Ti atoms in isolated TiO_4 sites.[29,36] Therefore, the LMCT band at 47 600 cm^{-1} for the dehydrated 1% TiO_2/SiO_2 sample can be assigned to isolated TiO_4 species.[36−38] A red shift of 1000−6000 cm^{-1} of LMCT transitions for Ti silicalite and TiO_2-SiO_2 mixed oxides was also observed upon hydration.[29,37,38] These changes in LMCT transitions upon hydration/dehydration indicate that the coordination geometry and oxygenated ligands of isolated Ti cations are different in hydration and dehydration environments.

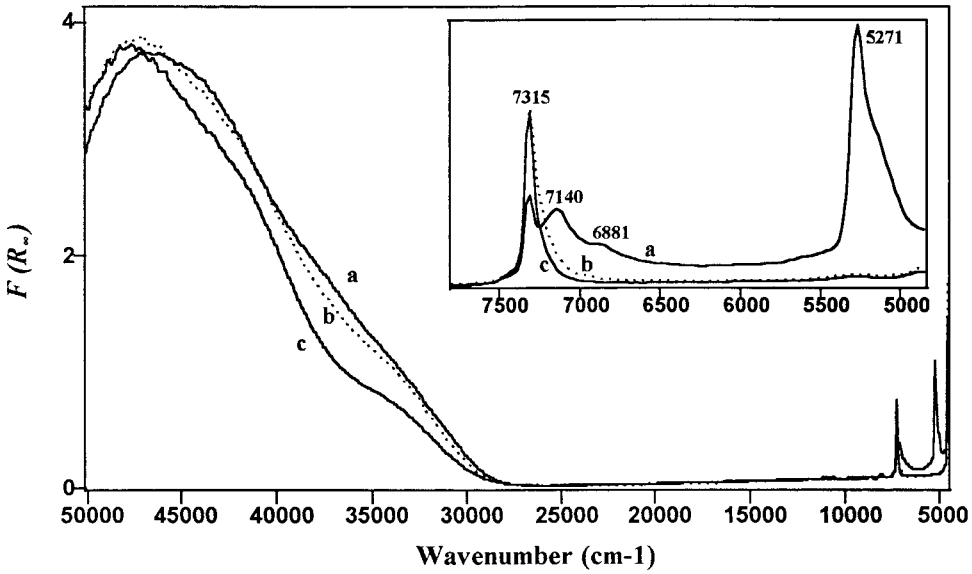

Figure 6. UV−vis−NIR DRS spectra of 1% TiO_2/SiO_2 under various conditions: (a) hydrated, (b) partially dehydrated at 120 °C, and (c) completely dehydrated at 500 °C.

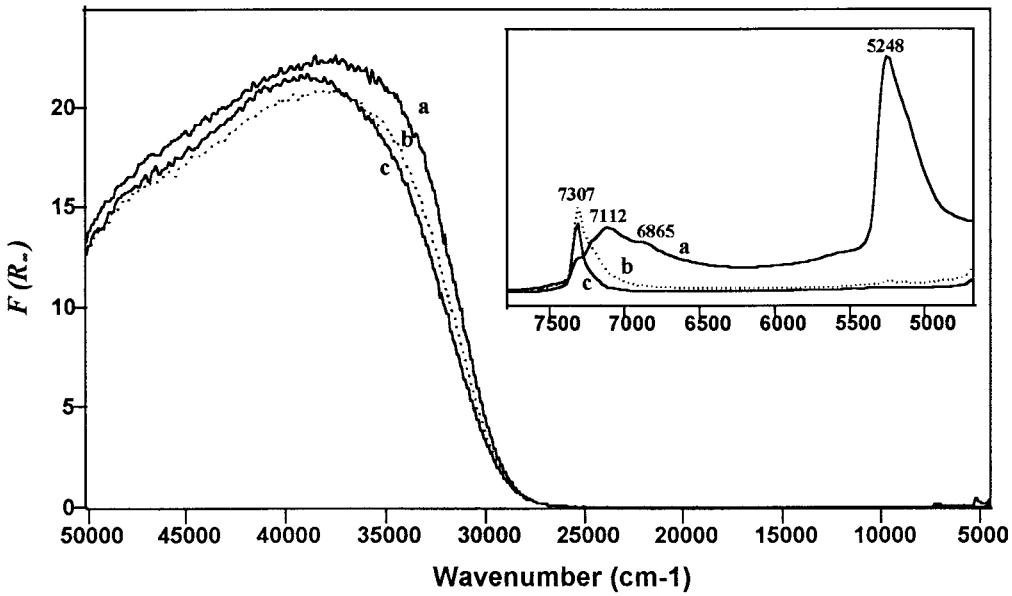

Figure 7. UV−vis−NIR DRS spectra of 12% TiO_2/SiO_2 under various conditions: (a) hydrated, (b) partially dehydrated at 120 °C, and (c) completely dehydrated at 500 °C.

The DRS spectra for 12% TiO_2/SiO_2 sample under similar conditions are shown in Figure 7. In the near-IR region, the hydrated sample possesses bands at 7315, 7112, 6865, and 5248 cm^{-1}, together with a weak shoulder at ∼7220 cm^{-1}. The three bands at 7112, 6865, and 5248 cm^{-1} are due to physisorbed H_2O molecules and disappear after partial dehydration, while the weak shoulder at ∼7220 cm^{-1} is still present. Complete dehydration significantly decreases the bands in the 7100−7300 cm^{-1} region. In the UV−vis region, partial dehydration slightly upward shifts the maximum LMCT band and complete dehydration shifts the band from 37 500 to 38 800 cm^{-1}.

The DRS spectra of the 30% TiO_2/SiO_2 sample under similar conditions are provided in Figure 8. In the near-IR region, the hydrated sample possesses bands at 7096, 6872, and 5230 cm^{-1}, together with two weak shoulders at ∼7310 and ∼7220 cm^{-1}. After the removal of physisorbed H_2O molecules by partial dehydration, the band at 7311 cm^{-1} and a strong shoulder at 7220 cm^{-1} become more pronounced. Complete dehydration results in the disappearance of the band at 7220 cm^{-1}, which most likely originates from the overtone stretching vibration of Ti−OH hydroxyls since pure TiO_2 possesses similar absorption at ∼7186 cm^{-1}. (See Figure 9 for the comparison of the DRS bands due to hydroxyl groups in different partially dehydrated samples.) In the corresponding UV−vis region, the DRS spectra of the 30% TiO_2/SiO_2 sample (see Figure 8) under hydrated and dehydrated conditions are almost identical, indicating that the coordination geometry of the Ti cations is saturated and not affected by the presence of H_2O molecules, which is similar to the behavior of bulk titanium oxide (anatase).

The DRS spectra of different TiO_2/SiO_2 samples under dehydrated conditions are compared in Figure 10. The LMCT transitions shift to lower wavenumbers with increasing TiO_2 loading, while the intensity of the 7315 cm^{-1} band due to isolated Si−OH hydroxyls decreases significantly, which indicates the consumption of Si−OH hydroxyls with increasing TiO_2 loading. As compared to Figure 9, the 7220 cm^{-1} band due to Ti−OH hydroxyls disappears after complete dehydration, indicating that most of Ti−OH hydroxyls are not stable and

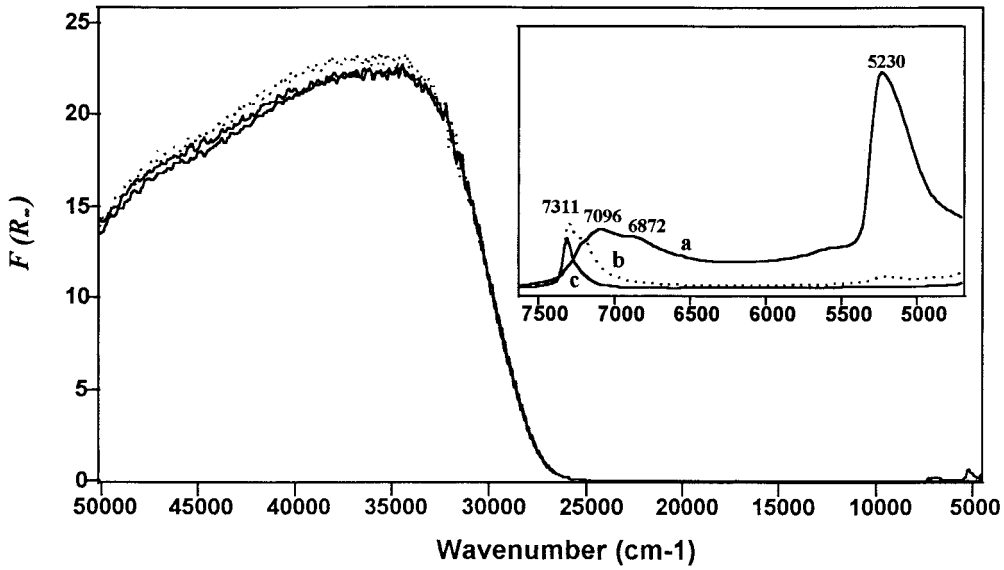

Figure 8. UV−vis−NIR DRS spectra of 30% TiO_2/SiO_2 under various conditions: (a) hydrated, (b) partially dehydrated at 120 °C, and (c) completely dehydrated at 500 °C.

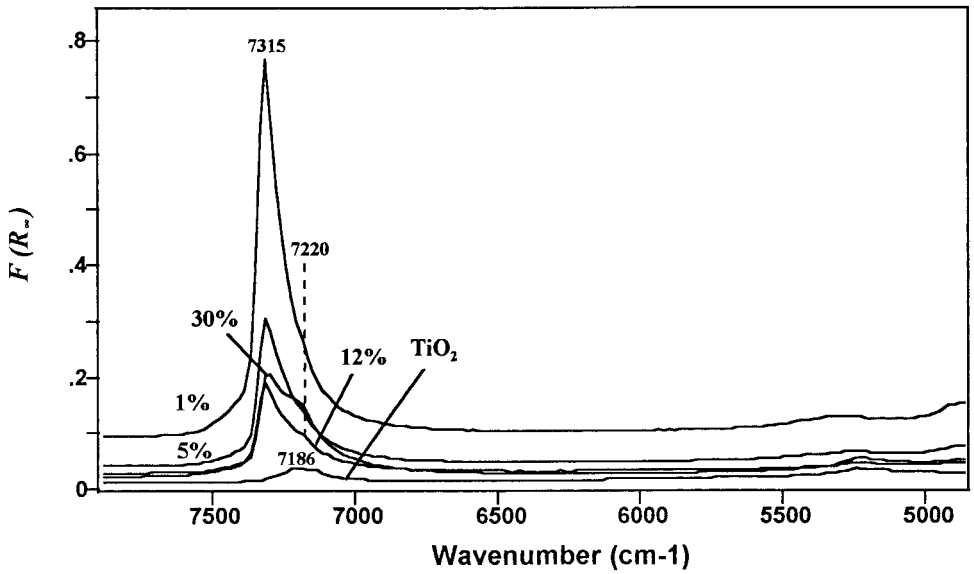

Figure 9. Comparison of NIR DRS spectra of pure TiO_2 (P-25) and TiO_2/SiO_2 at different loadings after partial dehydration at 120 °C.

dehydroxylated after the dehydration at 500 °C, in agreement with the results published by Haukka et al.[16] The relative intensities of hydroxyl groups on different samples with respect to pure silica are listed in Table 3. The intensity of Si−OH hydroxyls on the 12% TiO_2/SiO_2 sample is about the same as on the 30% TiO_2/SiO_2 sample, suggesting that the consumption of Si−OH groups by titanium oxide species has reached the limit by 12% TiO_2 (actual 14.75% TiO_2), which is consistent with the maximum dispersion of titanium oxide surface species at this loading (~4 Ti atoms/nm^2).

The maximum LMCT transitions and the corresponding band-gap energies of the hydrated and dehydrated TiO_2/SiO_2 samples are summarized in Table 4. The band-gap energy (E_g) for allowed transitions was determined by finding the intercept of the straight line in the low-energy rise of a plot of $[F(R_\infty)h\nu]^2$ against $h\nu$, where $F(R_\infty)$ is Kubelka−Munk function and $h\nu$ is the incident photon energy.[39] It was found that the increase of TiO_2 loading decreases the LMCT transitions and the edge position. It is interesting to note that although the DRS spectrum of 30% TiO_2/SiO_2 is different from that of pure TiO_2 (P-25), they possess the same band-gap energy of 3.60 eV. This result suggests that even though the TiO_2 crystallites in the 30% TiO_2/SiO_2 sample are very small that are beyond the detection sensitivity of XRD measurements, they may still possess the same electronic property as the pure TiO_2 (predominantly anatase) phase. For the highly dispersed TiO_2/SiO_2 samples, dehydration results in increased band-gap energies, but the effect on the 1% TiO_2/SiO_2 sample is relatively minor due to the isolation of Ti cations as will be discussed later. Nevertheless, dehydration does not affect the edge positions of 30% TiO_2/SiO_2 and pure TiO_2. The results demonstrate that, for the highly dispersed TiO_2/SiO_2 catalysts, either the removal of H_2O from the surface by partial dehydration at 120 °C or the dehydroxylation of Ti−OH and Si−OH hydroxyls by the complete dehydration at 500 °C changes the coordination environment of the surface Ti atoms.

The UV−vis−NIR DRS spectra are usually considered to provide information about the coordination geometry of the Ti cations (the first coordination sphere) and the change in ligands (the second coordination sphere) under various conditions. Jørgensen[40] proposed that the LMCT transitions between the ligand (X = H−O$^-$, Si−O$^-$, Ti−O$^-$, etc.) and the empty d

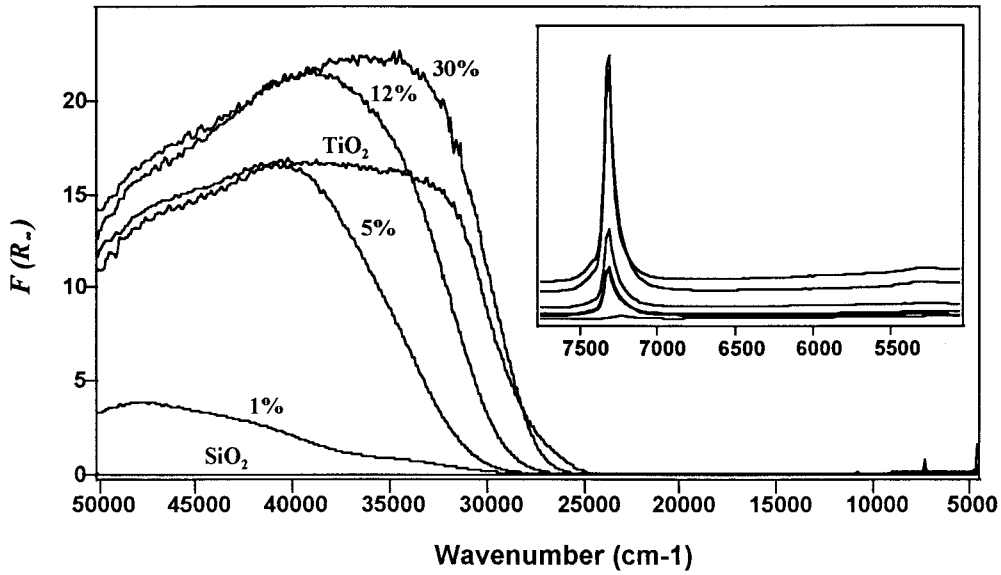

Figure 10. UV−vis−NIR DRS spectra of pure SiO_2, 1%−30% TiO_2/SiO_2, and pure TiO_2 after completely dehydration at 500 °C.

TABLE 3: Comparison of Hydroxyl Concentrations on Dehydrated TiO_2/SiO_2 Catalysts

catalysts	hydroxyl band (cm^{-1})	int ($F(R_\infty)$)	rel int[a]
SiO_2	7315	0.67	100
1% TiO_2/SiO_2	7315	0.65	97
5% TiO_2/SiO_2	7315	0.23	34
12% TiO_2/SiO_2	7315	0.13	20
30% TiO_2/SiO_2	7312	0.14	21
TiO_2	7235	0.008	1

[a] The relative intensity is the hydroxyl peak intensity ($F(R_\infty)$, Kubulk−Mounk function) of the sample relative to the hydroxyl peak intensity of SiO_2 as a reference of 100.

TABLE 4: Band Maximum and Edge Energy of Hydrated and Dehydrated TiO_2/SiO_2 Catalysts

catalysts	band max (cm^{-1}) (hyd)	E_g (eV) (hyd)	band max (cm^{-1}) (dehyd)	E_g (eV) (dehy)
1% TiO_2/SiO_2	46 600	4.66	47 600	4.68
5% TiO_2/SiO_2	38 200	3.88	40 400	4.19
12% TiO_2/SiO_2	37 200	3.78	38 800	3.84
30% TiO_2/SiO_2	34 500	3.60	34 500	3.60
TiO_2 (P-25)	32 000	3.60	32 000	3.60
TiO_2 (rutile)[a]	29 800	3.22		

[a] Obtained after calcining TiO_2 (P-25) at 850 °C for 2 h.

orbital of Ti^{4+} can be estimated from the optical electronegativities χ of ligand X and Ti^{4+} by the following equation:

$$\bar{\nu}\ (\mathrm{cm}^{-1}) = 30000[\chi_{\mathrm{opt}}(\mathrm{X}) - \chi_{\mathrm{opt}}(\mathrm{Ti})]$$

The increase of the coordination number of Ti from 4-fold to 6-fold increases the χ_{opt}(Ti) value from 1.85 to 2.05.[40] So, the LMCT band for Ti in octahedral sites is located at a lower wavenumber relative to Ti in tetrahedral sites. In Table 4, the LMCT transitions of TiO_2 (P-25) (predominantly anatase) were observed at 32 000 cm^{-1} with a band edge energy of 3.60 eV, while the LMCT transitions of TiO_2 (rutile) were observed at ~29 800 cm^{-1} with a band edge energy of 3.22 eV. Because the Ti atoms in either the anatase or rutile phase are located in octahedral sites, the results indicate that a single value of the optical electronegativity may not properly represent the Ti atoms in different coordination and ligand environments. Moreover, the electronegativity values used for oxygenated ligands having different second coordination spheres are quite arbitrary in the literature: Si−O^- ligand (χ_{opt} = 3.17) and H−O^- ligand (χ_{opt} = 2.9),[41] X−O^- ligands (χ_{opt} = 3.45, X = H−O^- and O^{2-}),[29,38] H_2O ligand (χ_{opt} = 3.5).[41] Therefore, the above equation cannot be quantitatively used to account for the shift of the LMCT transitions of the Ti atoms upon the change in coordination and ligand environments. This is further verified by the UV−vis−NIR DRS experiments of three Ti reference compounds that possess different coordination geometries and ligands, as shown in Figure 11. Ba_2TiO_4 possesses isolated TiO_4 tetrahedra linked by Ba atoms.[42] JDF-L1 ($Na_4Ti_2Si_8O_{22}\cdot 4H_2O$) and Ti umbite ($K_2TiSi_3O_9\cdot H_2O$) contain isolated TiO_5 square pyramids and isolated TiO_6 octahedra with Ti−O−Si linkages, respectively.[43,44] The LMCT transitions and edge energy of Ti cations decrease in the order JDF-L1 (4.66 eV) > Ti umbite (4.56 eV) > Ba_2TiO_4 (4.09 eV). This is in contrast to the expectation that Ba_2TiO_4 with 4-fold coordination would display the highest LMCT transitions. The actual lowest LMCT transitions of the Ti atoms in Ba_2TiO_4 can be accounted for by Ba atoms as the second coordination sphere that are much less electronegative than Si atoms as the second coordination sphere for Ti atoms in JDF-L1 and Ti umbite. The results demonstrate that the ligands can play a major role in determining the band maximum of the LMCT transitions of Ti cations.

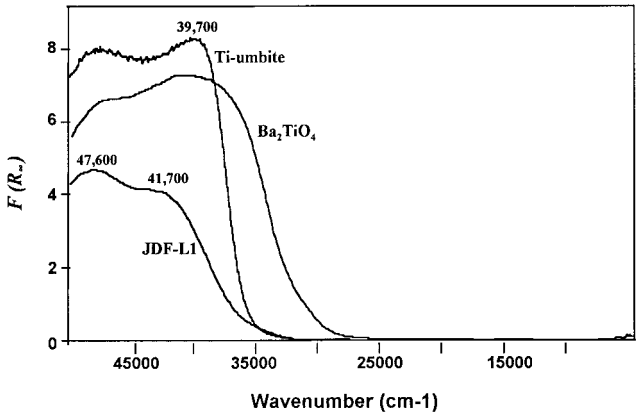

Figure 11. UV−vis−NIR DRS spectra of Ti reference compounds.

The hydration of the dehydrated 1%−12% TiO_2/SiO_2 samples causes only a slight red shift of the LMCT transitions, ~1000 cm^{-1}, indicating that coordination geometry change as well as any ligand change due to hydration has a relatively minor

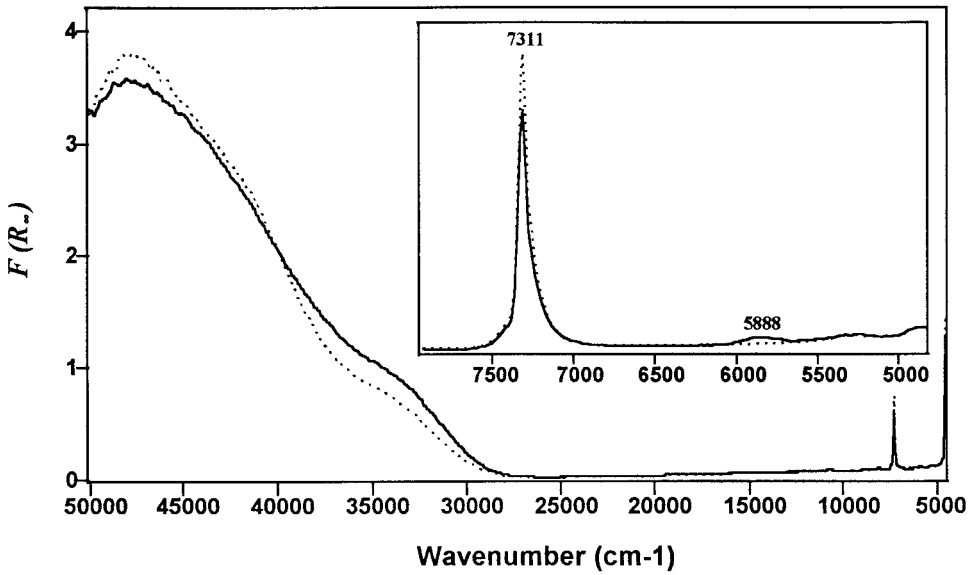

Figure 12. UV−vis−NIR DRS spectra of 1% TiO_2/SiO_2 after dehydration at 500 °C (dashed line) and methanol reaction at 230 °C (solid line).

TABLE 5: Effect of Methanol Reaction on the Band Edge Position and the Intensity of Hydroxyls

catalysts	band max (cm^{-1})	E_g (eV)	methoxy band (cm^{-1})	hydroxyl band (cm^{-1})	degree of hydroxyl reduction[a]
SiO_2			5888	7321	21
1% TiO_2/SiO_2	47 600	4.68	5888	7316	19
5% TiO_2/SiO_2	40 100	4.02	5885	7316	35
12% TiO_2/SiO_2	38 400	3.83	5882	7317	46
30% TiO_2/SiO_2	34 500	3.60	5870	7308	48
TiO_2	32 000	3.60	5783	7220	25

[a] Percentage of the intensity reduction (Kubulk−Mounk function) due to the formation of surface methoxy species with respect to the intensity of hydroxyls under completely dehydrated conditions.

contribution to the shift of the LMCT transitions. Thus, the significant red shift of the LMCT transitions and the decrease in the edge energy with increasing TiO_2 loading (Figure 10 and Table 4) are more likely contributed to the formation of Ti−O−Ti bonds. Weber[39] found that the edge energy of the LMCT transitions of Mo^{6+} in various Mo compounds decreases with increasing size of the molybdenum domain, i.e., the number of the next-nearest neighbors. Similarly, the decrease of the edge energy of LMCT transitions of Ti atoms with increasing Ti loading may also be associated with the increase in the number of nearest Ti atoms, which suggests the polymerization of the surface Ti atoms on the silica surface at higher TiO_2 loadings.

The spectral change during methanol oxidation for the 1% TiO_2/SiO_2 sample is illustrated in Figure 12. The methanol oxidation environment increases the relative band intensity of the lower LMCT transitions around 40 000−30 000 cm^{-1}, but the band maximum and edge energy of the titanium oxide species are not affected (see Table 5). In addition, the surface methoxy species are observed from the newly appeared peak at ∼5888 cm^{-1}, which can be assigned to the overtone stretching vibrations of methoxy species.[45] A similar band is also observed on the pure silica support (see Table 5); however, the band intensity is much weaker than on the 1% TiO_2/SiO_2 sample. These results suggest that the contribution to the band at 5888−5882 cm^{-1} for the highly dispersed TiO_2/SiO_2 samples may come from both Si−methoxy and Ti−methoxy species, in agreement with the in-situ Raman results. The reduced intensity of the 7315 cm^{-1} band due to Si−OH hydroxyls also indicates the involvement of Si−OH hydroxyls in the formation of the surface Si−methoxy species. The effects of the methanol oxidation environment on the DRS spectra of the 1%−30% TiO_2/SiO_2 samples, as well as pure TiO_2 (P-25), are summarized in Table 5. The changes in the band maximum and edge energy of the 5% TiO_2/SiO_2 sample are relatively significant, but for the 12% TiO_2/SiO_2 sample the changes are minor. No changes in the DRS spectra in the UV−vis region were observed for the 30% TiO_2/SiO_2 and pure TiO_2 samples during methanol oxidation.

5. X-ray Absorption Spectroscopy (XANES). The Ti K-edge XANES spectra of 1% and 12% TiO_2/SiO_2 under hydrated and dehydrated conditions are presented in Figure 13. The pre-edge features of both samples show significant differences between the two conditions, with the peak intensity in the dehydrated state being significantly higher, suggesting that the average coordination number of Ti atoms is lower in the dehydrated state.

To estimate the coordination of Ti atoms, the pre-edge peak intensities of 1% and 12% TiO_2/SiO_2 samples under hydrated and dehydrated conditions were plotted against the peak energy in Figure 14, together with the literature Ti compounds for comparison.[46] Farges et al.[46] found that pre-edge peak energies and heights for Ti model compounds fall into three well-separated domains according to their coordination geometry, as shown in Figure 14. The upper left domain is 4-fold coordinated, while the lower right domain is 6-fold coordinated and the middle domain is 5-fold coordinated. According to Farges et al., both the pre-edge position and the normalized height should be used to correctly determine the Ti coordination number. The TiO_2/SiO_2 supported oxides do not locate within the three domains but fall to the left side of the three domains with lower edge energy and height. For example, the peak height of the hydrated 12% TiO_2/SiO_2 sample is characteristic of 6-fold coordination; however, its pre-edge energy is ∼1 eV lower than the center of the 6-fold coordination domain. The results suggest that the pre-edge features must be mixtures of at least two Ti coordinations. From the comparison with the

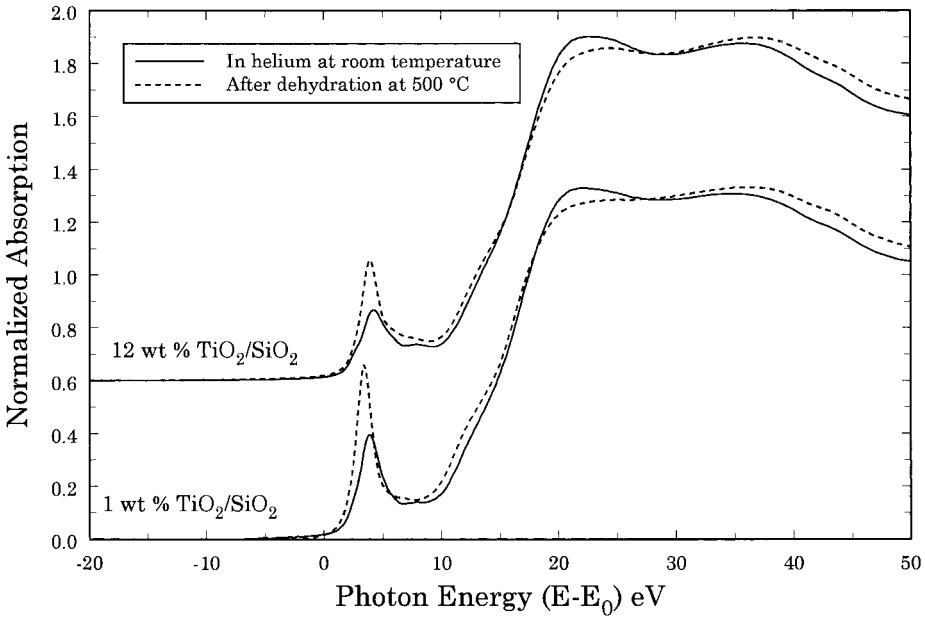

Figure 13. Ti K-edge XANES spectra of 1% and 12% TiO_2/SiO_2 samples in the hydrated state (solid line) and after dehydration at 500 °C (dashed line). (The spectra for the 12% TiO_2/SiO_2 sample are offset vertically for clarity.)

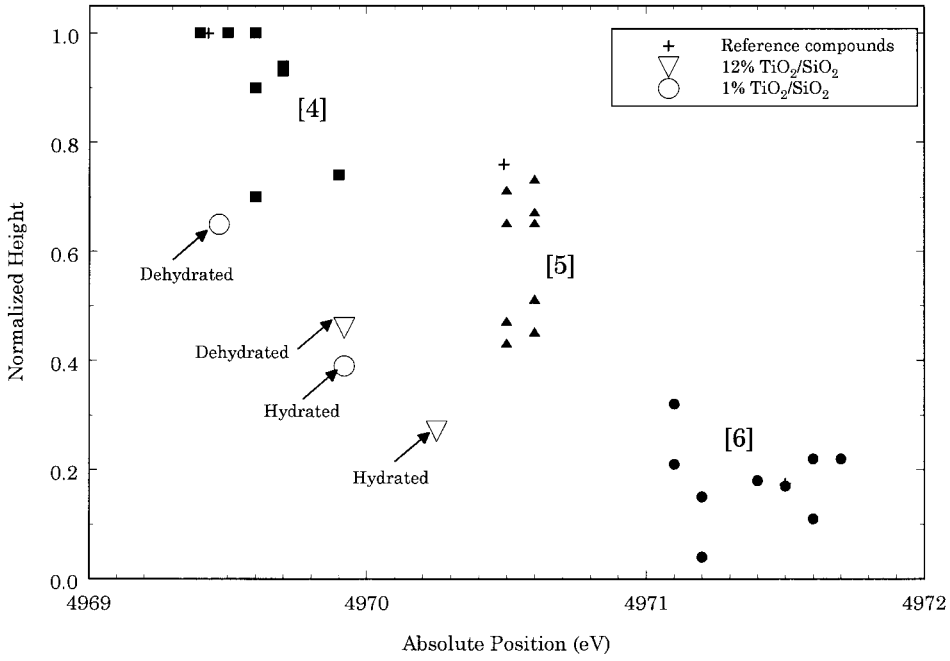

Figure 14. Comparison of the pre-edge energies and heights of the hydrated and dehydrated TiO_2/SiO_2 samples with reference compounds. (The data for the reference compounds were taken from ref 46. Our data for Ba_2TiO_4 (4-fold), fresnoite (5-fold), and anatase (6-fold) are indicated by the + symbols. These data are in excellent agreement with Farges et al.)

predicted values for different mixtures between 4-, 5-, and 6-fold coordinated Ti by Farges et al.,[46] it is estimated that in the dehydrated 1% TiO_2/SiO_2 sample the coordination of Ti is predominantly 4-fold (possibly mixed with a very small amount of 6-fold and/or 5-fold coordination). Upon hydration, the average coordination number increases, with predominantly 5-fold coordination mixed with some 4-fold and possibly a very small amount of 6-fold coordination. However, the Ti atoms in the dehydrated 12% TiO_2/SiO_2 sample are predominantly 5-fold coordinated, and hydration increases their coordination mostly to 6-fold. These estimated results are presented in Table 6.

TABLE 6: Estimation of Ti Coordination from Pre-edge Peak Energy and Height of Ti K-Edge XANES

catalyst	dehydrated[a]	hydrated
1% TiO_2/SiO_2	$[4]_p + [6]_{vm}/[5]_{vm}$	$[5]_p + [4]_m/[6]_{vm}$
12% TiO_2/SiO_2	$[5]_p + [4]_m/[6]_{vm}$	$[6]_p + [5]_{vm}/[4]_{vm}$

[a] Subscripts: p = predominant, m = minor, and vm = very minor.

6. Methanol Oxidation Reaction. The activity and selectivity of the TiO_2/SiO_2 supported oxides for methanol oxidation are presented in Table 7. The pure silica support does not show any detectable activity under the same reaction condition. For the highly dispersed 1%−12% TiO_2/SiO_2 catalysts, a very high selectivity (≥92%) to redox products, formaldehyde and methyl formate (MF), was observed. However, the TOF of the surface titanium oxide species dramatically decreases as the TiO_2

TABLE 7: Activity and Selectivity of TiO_2/SiO_2 Catalysts for Methanol Oxidation at 290 °C

			selectivity (%)			
catalyst	Ac[a]	TOF[b]	HCHO	MF	DMM	DME
1% TiO_2/SiO_2	28	63	56	44	0	0
5% TiO_2/SiO_2	49	22	55	44	1	0
8% TiO_2/SiO_2	32	9	58	37	3	3
12%TiO_2/SiO_2	17	3	63	29	2	6
30%TiO_2/SiO_2	7		0	29	0	71
TiO_2 (P-25)	3		0	0	0	100

[a] In millimoles of methanol converted per gram catalyst per hour. [b] Turnover frequency (TOF, 10^{-3} s^{-1}) is calculated on the basis of the total Ti atoms in the molecularly dispersed catalyst for the production of HCHO (formaldehyde) + MF (methyl formate)+DMM (dimethoxy methane).

TABLE 8: Activity and Selectivity of the 12% TiO_2/SiO_2 Sample at Different Temperatures

reaction *T*	conversion		selectivity (%)			
(°C)	(%)	Ac[a]	HCHO	MF	DMM	DME
290	5.5	17	63	29	2	6
310 (15 min)	10.4	32	54	37	2	7
310 (2 h)	4	12	38	35		27
350	7.6	23	24	24		52

[a] In millimoles of methanol converted per gram catalyst per hour.

loading increases from 1% to 12%, indicating that the reactivity of the highly dispersed TiO_2/SiO_2 catalysts is a strong function of the TiO_2 loading. On the contrary, the pure TiO_2 phase produces only dimethyl ether (dehydration product) and exhibits a very low activity for methanol oxidation. The 30% TiO_2/SiO_2 catalyst also exhibits a low reactivity and a high selectivity to dimethyl ether, which supports the Raman results that a large amount of small TiO_2 crystallites (anatase) are present on this sample.

The 12% TiO_2/SiO_2 sample, possessing the maximum dispersion of titanium oxide, was further tested for any rapid deactivation during methanol oxidation at higher tempertaures. The activity and selectivity are illustrated in Table 8. The 12% TiO_2/SiO_2 catalyst was not stable during the reaction since longer reaction times and higher reaction temperatures significantly decrease the selectivity of the redox products and increase the selectivity of the dehydration product, suggesting that TiO_2 crystallites may be formed during the reaction. This is further confirmed by Raman spectroscopy, which shows the formation of TiO_2 crystallites (anatase) on the used 12% TiO_2/SiO_2 catalyst after the reaction.

Discussion

Factors Controlling the Dispersion of Surface Titanium Oxide Species on the SiO_2 Support. The silica surface is known to be inert relative to other oxide supports, and consequently, monolayer dispersion of surface titanium oxide species on silica is very difficult to reach, with many factors governing the dispersion capacity of the silica surface. The structure of the SiO_2 surface is known to terminate in either siloxane groups with the oxygen on the surface (≡Si−O−Si≡) or one of the three types of hydroxyls: isolated hydroxyls (≡Si−OH), H-bonded hydroxyls (≡Si−O−H···OH−Si≡), and geminal hydroxyls (=Si$(OH)_2$).[30] Chemical surface modification reactions on silica usually involve the surface hydroxyls because the siloxane bridges are relatively unreactive with most molecules.[30] The consumption of Si−OH hydroxyls during deposition of titanium oxide on the silica support is confirmed by both DRS and Raman spectroscopy.

The highest concentration of hydroxyls on the silica surface is preferred in order to prepare high surface coverage of molecularly dispersed TiO_2/SiO_2 catalysts and is best realized at low temperatures. However, the silica surface also possesses a large amount of physisorbed water at room temperature, which will hydrolyze the Ti isopropoxide precursor to form crystalline TiO_2 and must be removed prior to introduction of the Ti isopropoxide precursor. The complete removal of physisorbed water at 120 °C was verified by the NIR DRS spectra. Thus, a pretreatment temperature of 120 °C was used to remove the physisorbed water as well as to preserve the highest amount of hydroxyls on the silica surface.

The reaction time is also an important experimental parameter in determining the overall conversion of surface hydroxyls that react with the reactive H-sequestering agents. Prolonged reaction time significantly enhances the reaction degree of the surface hydroxyls, especially for the less reactive H-bonded hydroxyls.[47,48] Washing away the reagent, after a short period following impregnation, does not result in high loading because of the incomplete reaction of the silica surface hydroxyls with the reagents. Thus, in the preparation procedure employed in the present investigation, the impregnated samples were kept under a N_2 flow for overnight because the prolonged impregnation time ensured complete reaction between the reagent and the surface hydroxyls as well as removing most of the solvent.

Another critical factor, that is rarely addressed in the literature, regarding the preparation of highly dispersed TiO_2/SiO_2 catalysts is the maximum surface coverage of the precursor molecules. By studying the reaction of a variety of reactive hydrogen-sequestering reagents with the silica surface, Morrow and Mcfarlan[17] found that the number of inaccessible hydroxyls and the number of H-bonded hydroxyls that do not react increase with the apparent size of the reactant precursor molecule. A large chemisorbed precursor molecule can block other hydroxyls and prevent them from reacting. In addition, the porosity, size, and morphology of the silica pores may influence the maximum surface coverage of a precursor. Very small pores may be inaccessible to large precursor molecules. Therefore, the maximum surface coverage of the precursor molecules is associated with the sterical hindrance effect.[30] Above the maximum surface coverage, extra precursor molecules do not react with the surface hydroxyls and remain on the surface after the solvent is removed. The unreacted precursor molecules either evaporate during calcination at elevated temperatures or remain on the surface and become oxidized into a crystalline oxide phase. In the current preparation, due to the sterical hindrance effect, the maximum surface coverage of the Ti(O−Pr^i)$_4$ precursor in a one-step impregnation was found to be ∼2.5 Ti atoms/nm^2, which is similar to the maximum trimethylsilyl (TMS) surface coverage of 2.2−2.7 groups/nm^2.[30,49]

The above discussion suggests that the availability and reactivity of the surface hydroxyl groups determine the maximum coverage of an organometallic precursor for a one-step impregnation reaction. However, after calcination some of the Si−OH groups become reexposed and can further react with more Ti(O−Pr^i)$_4$ precursor molecules. Thus, a higher loading of 12% TiO_2/SiO_2 (actual amount of 14.75 wt %), which corresponds to ∼4 Ti atoms/nm^2, is reached by employing two impregnation steps.

The theoretical monolayer coverage of titanium oxide on silica has been estimated to be ∼10 Ti/nm^2 based on the surface Ti density of the crystalline TiO_2 (anatase) (101) plane[1] or 5.5 Ti/nm^2 based on the surface Ti density of the TiO_2 (anatase) (010) plane.[50] However, the present results show that the

structure of the surface titanium oxide on silica is very different from that of crystalline TiO_2 (anatase), as in the case of other supported metal oxides.[51] Thus, the surface of TiO_2 (anatase), possessing close-packed and polymeric octahedral Ti cations, does not appear to be a reasonable reference for the silica-supported surface titanium oxide species. During the impregnation process, when the silica surface is fully covered with H-bonded hydroxyls, the $Ti(O-Pr^i)_4$ precursor should mostly react with these surface hydroxyls with a concentration of 4−5 OH/nm^2,[30] which is in agreement with the maximum loading of ∼4 Ti atoms/nm^2 found in the present study. Thus, this maximum dispersion is considered as the experimental monolayer coverage of surface titanium oxide species on silica supports.

Although the siloxane bridges form hydrophobic regions on the silica surface that cannot act as anchoring sites for reagents at low temperatures, higher temperatures can activate siloxane bridges to react with chlorosilanes, ammonia, $TiCl_4$, and $AlMe_3$,[16,30,52,53] which may result in the cleavage of some surface siloxane bridges. Thus, a high calcination temperature of 500 °C may cleave the surface siloxane bridges, which will become available for further bonding with the metal cations that are already anchored on the surface via surface hydroxyls from the prior low-temperature impregnation step. The red shift and intensity reduction of the Raman band at 802 cm^{-1}, due to the Si−O−Si stretching mode, are indicative of breaking of some Si−O−Si bridges during high-temperature calcination. Raman bands at ∼919 and ∼1080 cm^{-1}, due to Ti−O−Si bonds, may also partially contribute to breaking of some Si−O−Si bridges during the formation of the surface titanium oxide species. These results suggest that during calcination both the surface hydroxyl groups and the cleaved siloxane bridges can participate in bonding with the surface titanium oxide species to form Ti−O−Si bonds on the SiO_2 surface. Thus, the silica surface is significantly modified by the supported titanium oxide surface species.

Surface Structures of Molecularly Dispersed TiO_2/SiO_2 under Various Conditions. The understanding of the coordination geometry of the Ti cations under various conditions is of great importance not only from the structural point of view but also for its correlation with the corresponding catalytic properties. The surface structures of molecularly dispersed TiO_2/SiO_2 supported oxides under hydrated conditions and dehydrated conditions and during methanol oxidation were extensively investigated by in-situ Raman, UV−vis−NIR DRS, and XANES spectroscopies in the current study.

Investigation of the dehydrated structure of the supported surface metal oxide species is crucial for fully understanding catalytic reaction mechanisms because most of the oxidation reactions occur at high temperatures where the real working catalysts are under dehydrated conditions. In the dehydrated state, Raman spectroscopy and XPS indicate the formation of Ti−O−Si bridging bonds on the silica surface. The DRS results alone are insufficient to determine the coordination of Ti atoms because of the mixed contribution to the LMCT transitions from both the coordination and the ligands. Combining the in-situ DRS and XANES spectroscopies provides the direct and reliable structural information about the surface titanium oxide species. Both DRS and XANES spectroscopies reveal that the Ti atoms in the dehydrated 1% TiO_2/SiO_2 sample are predominantly composed of isolated TiO_4 sites. However, in the DRS spectra of the dehydrated 1% TiO_2/SiO_2 sample (Figure 10), two weak shoulders at ∼40 600 and ∼34 000 cm^{-1} are also present besides the dominant band at 47 600 cm^{-1}. Trong On et al.[37] observed a LMCT band at 40 900 cm^{-1} for the 1.5% TiO_2-SiO_2 gel, which they thought to originate from TiO_4 sites. However, compared to the LMCT band of the truly isolated TiO_4 sites in TS-1, which they observed at ∼50 000 cm^{-1},[37] the 9100 cm^{-1} difference in the LMCT band is very significant. It is currently proposed that the LMCT band at ∼40 600 cm^{-1} might be due to $O_3Ti-O-TiO_3$ dimers and/or TiO_4 units connected in one-dimensional polymerized chains with one or two nearest Ti neighbors for each Ti atom. Therefore, the Ti atoms in the dehydrated 5% TiO_2/SiO_2 sample may be dominant with O_3-Ti−O−TiO_3 dimers and/or one-dimensional polymerized TiO_4 units since its LMCT band is at ∼40 400 cm^{-1}.

The LMCT band for the dehydrated 12% TiO_2/SiO_2 sample is at ∼38 800 cm^{-1}, while XANES spectra reveal that the Ti atoms predominantly possess 5-fold coordination (Table 6). These results suggest that the surface Ti species on the dehydrated 12% TiO_2/SiO_2 sample might be two-dimensional, polymerized TiO_5 units since no TiO_2 crystallites (anatase) were observed on this highly dispersed sample by Raman spectroscopy. The two-dimensional, surface polymeric TiO_5 units in the dehydrated state possess at least one Ti−O−Si bond and three or more Ti−O−Ti bonds. A small amount of polymerized TiO_6 species are also possibly present as suggested by the XANES analysis (Table 6), which may contribute to the LMCT band at ∼34 000 cm^{-1}. In summary, (1) the LMCT band at 47 600 cm^{-1} is associated with Ti atoms in the isolated TiO_4 sites, (2) the LMCT band at 40 600 cm^{-1} is assigned to Ti atoms in dimeric or one-dimensional, polymerized TiO_4 units, (3) the LMCT band at ∼39 000 cm^{-1} is assigned to two-dimensional, polymerized TiO_5 units, and (4) the LMCT band at 34 000 cm^{-1} is related to the polymerized TiO_6 units with the highest number of next-nearest Ti neighbors. In addition, the relative amounts of each dehydrated surface titanium oxide species is a strong function of Ti loading: the higher the Ti loading, the higher the degree of polymerization of the Ti oxide surface species and the higher the average coordination number of the Ti atoms. Thus, the surface Ti species on the dehydrated 1% TiO_2/SiO_2 sample contain predominantly isolated TiO_4 units, and the surface Ti species on the dehydrated 5% TiO_2/SiO_2 sample mainly consist of dimeric or one-dimensional polymerized TiO_4 units. For the dehydrated 12% TiO_2/SiO_2 sample, the surface Ti species are dominantly two-dimensional, polymerized TiO_5 units.

Moisture has a very pronounced effect on the surface structure of the highly dispersed titanium oxide species on silica. Hydration can break the Ti−O−Si bridging bonds, which result in the formation of Ti−OH as well as Si−OH that may be perturbed by the nearby Ti cation. The Raman band at 940−960 cm^{-1} is most likely due to the Ti perturbed Si−OH. Hydration also shifts the LMCT band to lower wavenumbers, indicating an increase in the average coordination number of the Ti cations. The presence of IR overtone bands in the region of 7315−7200 cm^{-1} due to Ti−OH hydroxyls in the partially hydrated state also supports that Ti−OH hydroxyls may originate from Ti−O−Si bonds. XANES analysis demonstrates that the coordination of the Ti atoms on the dehydrated 1% TiO_2/SiO_2 sample predominantly changes from 4 to 5 upon hydration and that the coordination of the Ti atoms on the 12% TiO_2/SiO_2 sample predominantly changes from 5 to 6 upon hydration. Thus, hydration appears to increase the average coordination number of the surface Ti cations by 1. The pre-edge peak intensity of the dehydrated 12% TiO_2/SiO_2 is slightly higher than that of the hydrated 1% TiO_2/SiO_2, suggesting that the average coordination number should be slightly lower in the dehydrated 12% TiO_2/SiO_2 sample. However, the LMCT

transitions of the dehydrated 12% TiO_2/SiO_2 sample are much lower than that of the hydrated 1% TiO_2/SiO_2 sample, indicating that the red shift of the LMCT peak most likely originates from the polymerization of surface Ti oxide species as discussed above. Furthermore, it should be noted that hydration of the dehydrated 1% TiO_2/SiO_2 sample does not influence the edge energy of the LMCT band (Table 4), which indicates that hydration does not produce more Ti−O−Ti bonds on this low loading sample. This result further confirms that the surface Ti atoms on 1% TiO_2/SiO_2 are predominantly isolated. On the contrary, hydration increases the edge energies of higher loading samples, 5% and 12% TiO_2/SiO_2, suggesting an increase in both the average coordination number and the total number of Ti−O−Ti bonds. Similarly, Klein et al.[38] also observed an increasing tendency for the formation of Ti−O−Ti bonds through hydration at higher Ti contents in the mixed TiO_2-SiO_2 oxides.

The structural changes of the surface Ti species on the silica support during methanol oxidation were examined by in-situ UV−vis−NIR DRS and Raman spectroscopies. The Raman and DRS studies reveal that some ligands of the Ti cations (Ti−OSi or Ti−OH) are converted to $Ti-OCH_3$ due to methanol chemisorption. The coordination geometry of the surface Ti atoms on the 1%−12% TiO_2/SiO_2 samples may only be slightly affected since very minor changes in the maximum of the LMCT transitions were observed due to methanol adsorption (see Table 5). In analogy to the hydrolysis of Ti−O−Si by H_2O molecules, a methanol molecule may also break a Ti−O−Si bond, forming either $Ti-OCH_3$ and Si−OH or $Si-OCH_3$ and Ti−OH. In either case, the recombination of $Ti-OCH_3$ and Si−OH or Ti−OH and $Si-OCH_3$ seems less favorable than the recombination of Ti−OH and Si−OH because of the higher stability of the surface methoxy intermediates. During methanol oxidation, the surface titanium oxide species, especially at high loadings, aggregate and form TiO_2 crystallites. This observation supports the conclusion that the chemisorption of methanol molecules breaks the Ti−O−Si bridging bonds and facilitates the aggregation of the surface titanium oxide species on the silica surface.

Fundamental Relationship between Structural Characteristics and Catalytic Properties of the Molecularly Dispersed TiO_2/SiO_2 Catalysts. The function of a support is primarily known to tailor the catalytic performance of the active component by (1) altering the exposure or dispersion of the active sites and (2) modifying their nature through interaction with the underlying support. The catalytic performance of titanium oxide appears to be completely modified by its interaction with the silica support, which is associated with changes in the molecular structure and coordination environments. The unique catalytic performance of the highly dispersed TiO_2/SiO_2 catalysts in comparison with TiO_2 crystallites was previously demonstrated for liquid-phase epoxidation reactions.[8] The pure TiO_2 phase is not active for the epoxidation reaction, and the highly dispersed TiO_2/SiO_2 catalysts exhibit high reactivity and high epoxide selectivity.[8] In the present study, the pure TiO_2 crystallites also display no significant activity for methanol oxidation and are nonselective to the redox products (formaldehyde and methyl formate). In contrast, the molecularly dispersed TiO_2/SiO_2 catalysts are much more active for methanol oxidation and are highly selective to the redox products. In addition, the catalytic activity of methanol oxidation on the molecularly dispersed TiO_2/SiO_2 catalysts is also a strong function of TiO_2 loading, which is associated with changes in the coordination geometry and the degree of polymerization of the surface Ti atoms. Although all the surface titanium oxide species on the silica support are highly selective to the redox products (selectivity >92%), the specific catalytic activity (TOF) of the different surface Ti species decreases in the order isolated TiO_4 species > polymerized TiO_4 species > polymerized TiO_5 species.

The highest TOF for the 1% TiO_2/SiO_2 sample indicates that the isolated TiO_4 sites are most active for methanol oxidation, which suggests that the site isolation in association with the maximum number of Ti−O−Si bridging bonds per Ti atom is most favorable for methanol oxidation. The observation of the surface Ti−methoxy species resulting from the breaking of the Ti−O−Si bridging bonds strongly supports the conclusion that methanol oxidation involves participation of Ti−O−Si bonds. For liquid-phase olefin epoxidation with alkyl hydroperoxide, the catalytic activity of mixed TiO_2-SiO_2 oxides has also been strongly correlated with the Ti−O−Si connectivity or the relative proportions of Ti−O−Si to Ti−O−Ti bonds.[54,55] The isolated TiO_4 sites provide the maximum number of Ti−O−Si bonds and, consequently, exhibit the highest specific catalytic activity for both methanol oxidation and olefin epoxidation reactions. Polymerization of the surface Ti atoms on the supported TiO_2/SiO_2 catalysts decreases the fraction of Ti−O−Si bonds and, therefore, significantly decreases the activity of the Ti active sites.

The production of redox products instead of the dehydration product (dimethyl ether) suggests an increased oxidizing potential and a decreased acidity of the Ti cations when dispersed on the silica support. Alcohol dehydration is known to be catalyzed by both Lewis and Brönsted acid sites and is considered as a measure for total acidity.[21,56,57] In the mixed TiO_2-SiO_2 oxides, the acidity, in terms of both density and strength, generally decreases with increasing Si content over the whole composition range.[21,56,58] The pure TiO_2 phase, possessing only Lewis acid sites,[9] catalyzes methanol dehydration to dimethyl ether. Therefore, the surface titanium oxide species on the silica support possess a lower acidity relative to the pure TiO_2 phase since the reaction products are exclusively redox products. The fact that the surface Ti cations on silica act as redox sites rather than acid sites also suggests an increased oxidizing potential of the Ti cations. The increased oxidizing potential of the Ti(IV) cations, due to the formation of Ti−O−Si bonds, is reflected in the increased BE values of Ti $2p_{3/2}$ and O 1s and the higher LMCT transitions of the Ti atoms in the molecularly dispersed TiO_2/SiO_2 catalysts. In addition, the Ti(IV) cations must be involved in a change in the oxidation state during the redox cycle of methanol oxidation. However, the details of the reaction mechanism over the molecularly dispersed TiO_2/SiO_2 supported oxides, which involves methanol chemisorption and the surface Ti−methoxy species decomposition steps, are not clear at the present time. Further investigation, in association with other oxidation reactions such as epoxidation reactions, may be necessary to provide additional fundamental insight into the relationship between the structural characteristics and the reactivity property of this type of catalyst.

Conclusions

Several factors are shown to be critical in controlling the dispersion capacity or the maximum surface coverage of surface titanium oxide species on silica: the concentration of surface hydroxyls on silica, the pretreatment temperature, the impregnation time, and the maximum surface coverage of the precursor molecules. Experimental monolayer dispersion of titanium oxide on silica (Cabosil EH-5) is reached at ~4 Ti atoms/nm^2 by employing a two-step impregnation procedure, which overcomes the limitation of the maximum coverage of precursor molecules on the silica surface in the one-step impregnation.

The results obtained by combined in-situ Raman, XPS, UV−vis−NIR DRS, and XANES spectroscopies are very informative for fundamental understanding of surface structures of the molecularly dispersed TiO_2/SiO_2 supported oxides under various conditions. The surface structures of these TiO_2/SiO_2 samples are found to be very sensitive to different environments/pretreatment. In the dehydrated state, for a low loading of 1% TiO_2, the surface Ti atoms are predominantly located at isolated TiO_4 sites; while at a medium loading of 5% TiO_2, the silica surface may possess a higher amount of TiO_4 dimer or one-dimensional, polymerized TiO_4 species; and at monolayer coverage (actual 14.75% TiO_2), two-dimensional, polymerized TiO_5 species are predominantly present on the silica surface. Upon hydration, some of the Ti−O−Si bridging bonds on these molecularly dispersed TiO_2/SiO_2 samples are hydrolyzed by H_2O molecules, which results in an increase in the average coordination number of the Ti cations by about 1. Hydration also decreases the edge energies of the LMCT transitions of the higher loading samples of 5% and 12% TiO_2/SiO_2, suggesting an increase in the total number of Ti−O−Ti bonds. Exposure to the methanol oxidation environment also breaks the Ti−O−Si bridging bonds, resulting in the formation of Ti−OCH_3 or Si−OCH_3 species.

The molecularly dispersed Ti cations on the silica surface act as redox sites rather than acid sites for methanol oxidation since the predominant reaction products are the redox products (formaldehyde and methyl formate). The TOF of the surface titanium oxide species significantly decreases with increasing TiO_2 loading, demonstrating that the reactivity of the surface Ti sites is a strong function of the molecular structural characteristics. Site isolation and the maximum number of Ti−O−Si bonds per Ti atom for isolated TiO_4 sites are responsible for the highest specific catalytic activity (TOF) of the 1% TiO_2/SiO_2 sample. Polymerization of the surface Ti species decreases the relative fraction of Ti−O−Si bonds and, therefore, significantly decreases the activity of the Ti active sites.

Acknowledgment. This work was funded by the U.S. National Science Foundation Grant CTS-9417981. The UV−vis−NIR DRS experiments were performed on a Varian Cary 5 UV−vis−NIR spectrometer that was supported by the U.S. Department of Energy, Basic Energy Sciences, Grant DE-FG02-93ER14350. Part of the research was carried out at the National Synchrotron Light Source, Brookhaven National Laboratory, which is supported by the U.S. Department of Energy, Division of Materials Sciences and Division of Chemical Sciences. We also thank Dr. K. Klier and Dr. B. Weckhuysen for helpful comments.

References and Notes

(1) Srinivasan, S.; Datye, A. K.; Smith, M. H.; Peden, C. H. F. *J. Catal.* **1994**, *145*, 565.
(2) Castillo, R.; Koch, B.; Ruiz, P.; Delmon, B. *J. Catal*. **1996**, *161*, 524.
(3) Mariscal, R.; Palacios, J. M.; Galan-Fereres, M.; Fierro, J. L. G. *Appl. Catal. A: Gen.* **1994**, *116*, 205.
(4) Galan-Fereres, M.; Mariscal, R.; Alemany, L. J.; Fierro, J. L. G. *J. Chem. Soc., Faraday Trans*. **1994**, *90*, 3711.
(5) Elguezabal, A. A.; Corberan, V. C. *Catal. Today* **1996**, *32*, 265.
(6) Dias, C. R.; Portela, M. F.; Galan-Fereres, M.; Banares, M. A.; Granados, M. L.; Pena, M. A.; Fierro, J. L. G. *Catal. Lett*. **1997**, *43*, 117.
(7) Sheldon, R. A.; Van Doorn, J. A. *J. Catal.* **1973**, *31*, 427.
(8) Sheldon, R. A. *J. Mol. Catal.* **1980**, *7*, 107.
(9) Deo, G.; Turek, A. M.; Wachs, I. E.; Huybrechts, D. R. C.; Jacobs, P. A. *Zeolites* **1993**, *13*, 365.
(10) Roark, R. D.; Kohler, S. D.; Ekerdt, J. G.; Kim, D. S.; Wachs, I. E. *Catal. Lett.* **1992**, *16*, 77.
(11) Roark, R. D.; Kohler, S. D.; Ekerdt, J. G. *Catal. Lett.* **1992**, *16*, 71.
(12) Castillo, R.; Koch, B.; Ruiz, P.; Delmon, B. *J. Catal*. **1996**, *161*, 524.
(13) Bond, G. C.; Tahir, S. F. *Appl. Catal*. **1991**, *71*, 1.
(14) Fernandez, A.; Leyrer, J.; Gonzalez-Elipe, A. R.; Munuera, G.; Knözinger, H. *J. Catal*. **1988**, *112*, 489.
(15) Srinivasan, S.; Datye, A. K.; Hampden-Smith, M.; Wachs, I. E.; Deo, G.; Jehng, J. M.; Turek, A. M.; Peden, C. H. F. *J. Catal*. **1991**, *131*, 260.
(16) Haukka, S.; Lakomaa, E.; Root, A. *J. Phys. Chem*. **1993**, *97*, 5085.
(17) Morrow, B. A.; Mcfarlan, A. J. *J. Non-Cryst. Solids* **1990**, *120*, 61.
(18) Klaas, J.; Schulz-Ekloff, G.; Jaeger, N. I. *J. Phys. Chem. B* **1997**, *101*, 1305.
(19) Bordiga, S.; Coluccia, S.; Lamberti, C.; Marchese, L.; Zecchina, A.; Boscherini, F.; Buffa, F.; Genoni, F.; Leofanti, G.; Petrini, G.; Vlaic, G. *J. Phys. Chem*. **1994**, *98*, 4125.
(20) Vayssilov, G. N. *Catal. Rev.—Sci. Eng*. **1997**, *39*, 209.
(21) Gao, X.; Wachs, I. E. *Catal. Today*, in press.
(22) Tatibouët, J. M. *Appl. Catal. A: Gen.* **1997**, *148*, 213.
(23) Jehng, J. M.; Hu, H.; Gao, X. T.; Wachs, I. E. *Catal. Today* **1996**, *28*, 335.
(24) Stakheev, A. Y.; Shpiro, E. S.; Apijok, J. *J. Phys. Chem*. **1993**, *97*, 5668.
(25) Mukhopadhyay, S. M.; Garofalini, S. H. *J. Non-Cryst. Solids* **1990**, *126*, 202.
(26) Brinker, C. J.; Kirkpatrick, R. J.; Tallant, D. R.; Bunker, B. C.; Montez, B. *J. Non-Cryst. Solids* **1988**, *99*, 418.
(27) MacMillan, P. *Am. Mineral*. **1986**, *69*, 622.
(28) Pei, S.; Zajac, G. W.; Kaduk, J. A.; Faber, J.; Boyanov, B. I.; Duck, D.; Fazzini, D.; Morrison, I. T.; Yang, D. S. *Catal. Lett*. **1993**, *21*, 333.
(29) Boccuti, M. R.; Rao, K. M.; Zecchina, Leofanti, A.; Petrini, G. *Stud. Surf. Sci. Catal*. **1989**, *48*, 133.
(30) Vansant, E. F.; Voort, P. V. D.; Vrancken, K. C. *Stud. Surf. Sci. Catal.* **1995**, *93*.
(31) Dutoit, D. C. M.; Schneider, M.; Baiker, A. *J. Catal*. **1995**, *153*, 165.
(32) Chmel, A.; Eranosyan, G. M.; Kharshak, A. A. *J. Non-Cryst. Solids* **1992**, *146*, 213.
(33) Salvado, I. M. M.; Navarro, J. M. F. *J. Non-Cryst. Solids* **1992**, *147&148*, 256.
(34) Perry, C. C.; Li, X.; Waters, D. N. *Spectrochim. Acta* **1991**, *47A*, 1487.
(35) Klein, S.; Thorimbert, S.; Maier, W. F. *J. Catal*. **1996**, *163*, 476.
(36) Grohmann, I.; Pilz, W.; Walther, G.; Kosslick, H.; Tuan, V. A. *Surf. Interface Anal.* **1994**, *22*, 403.
(37) Trong On, D.; Le Noe, L.; Bonneviot, L. *Chem. Commun*. **1996**, 299.
(38) Klein, S.; Weckhuysen, B. M.; Martens, J. A.; Maier, W. F.; Jacobs, P. A. *J. Catal*. **1996**, *163*, 489.
(39) Weber, R. S. *J. Catal*. **1995**, *151*, 470.
(40) Jϕrgensen, C. K. *Morden Aspectes of Ligand Field Theory*; North-Holland: Amsterdam, 1971.
(41) Duffy, J. A. *Struct. Bonding* (*Berlin*) **1977**, *32*, 147.
(42) Wu, K. K.; Brown, I. D. *Acta Crystallogr., Sect. B* **1973**, *29*, 2009.
(43) Roberts, M. A.; Sankar, G.; Thomas, J. M.; Jones, R. H.; Du, H.; Chen, J.; Pang, W.; Xu, R. *Nature* **1996**, *381*, 401.
(44) Lin, Z.; Rocha, J.; Brandao, P.; Ferreira, A.; Esculcas, A. P.; Pedrosa de Jesus J. D. *J. Phys. Chem. B* **1997**, *101*, 7120.
(45) Busca, G.; Elmi, A. S.; Forzatti, P., *J. Phys. Chem*. **1987**, *91*, 5263.
(46) Farges, F.; Brown, G. E., Jr.; Rehr, J. J. *Phys. Rev. B* **1997**, *56*, 1809.
(47) Van Der Voort, P.; Gillis-D'Hamers, I.; Vrancken, K. C.; Vansant, E. F. *J. Chem. Soc., Faraday Trans*. **1991**, *87*, 3899.
(48) Van Der Voort, P.; Gillis-D'Hamers, I.; Vansant, E. F. *J. Chem. Soc., Faraday Trans*. **1990**, *86*, 3751.
(49) Sindorf, D. W.; Maciel, G. E. *J. Phys. Chem*. **1982**, *86*, 5208.
(50) Munoz, A.; Munera, G. *Studies in Surface Science and Catalysis*; Poncelet, G., Jacobs, P. A., Grange, P., Delmon, B., Eds.; Elsevier: Amsterdam, 1991; Vol 63, p 627.
(51) Kung, H. H. *Stud. Surf. Sci. Catal*. **1989**, *45*, 103.
(52) Hair, M. L.; Hertle, W. *J. Phys. Chem.* **1969**, *73*, 2372.
(53) Voort Van Der, P.; Vranken, K. C.; Vansant, E. F. *J. Chem. Soc., Faraday Trans.* **1995**, *91*, 353.
(54) Hutter, R.; Mallat, T.; Baiker, A. *J. Catal*. **1995**, *153*, 177.
(55) Hutter, R.; Mallat, T.; Baiker, A. *J. Catal*. **1995**, *153*, 665.
(56) Doolin, P. K.; Alerasool, S.; Zalewski, D. J.; Hoffman, J. F. *Catal. Lett*. **1994**, *25*, 209.
(57) Kim, K. S.; Barteau, M. A.; Farneth, W. E. *Langmuir* **1988**, *4*, 533.
(58) Liu, Z.; Tabora, J.; Davis, R. J. *J. Catal*. **1994**, *149*, 117.